

Two-subband electron transport in nonideal quantum wells

O. G. Balev

*Departamento de Física, Universidade Federal de São Carlos,
13565-905, São Carlos, Brazil and Institute of Semiconductor Physics,
National Academy of Sciences, 45 Pr. Nauky, Kiev, 252650, Ukraine*

F. T. Vasko

*Departamento de Física, Universidade Federal de Mato Grosso do Sul,
79070-900, Campo Grande, Brazil and Institute of Semiconductor Physics,
National Academy of Sciences, 45 Pr. Nauky, Kiev, 252650, Ukraine*

Flávio Aristone

*Departamento de Física, Universidade Federal de Mato Grosso do Sul,
79070-900 Campo Grande, Brazil*

Nelson Studart

*Departamento de Física, Universidade Federal de São Carlos,
13565-905, São Carlos, Brazil
(February 28, 2000)*

Electron transport in nonideal quantum wells (QW) with large-scale variations of energy levels is studied when two subbands are occupied. Although the mean fluctuations of these two levels are screened by the in-plane redistribution of electrons, the energies of both levels remain nonuniform over the plane. The effect of random inhomogeneities on the classical transport is studied within the framework of a local response approach for weak disorder. Both short-range and small-angle scattering mechanisms are considered. Magnetotransport characteristics and the modulation of the effective conductivity by transverse voltage are evaluated for different kinds of confinement potentials (hard wall QW, parabolic QW, and stepped QW).

PACS 73.20.Dx; 73.40.-c; 72.10.Fk

I. INTRODUCTION

The study of transport properties of semiconductor structures with many occupied electronic subbands has attracted scientific interest for a long time, concerning especially with two-subband occupancy and screening effects in the scattering processes [1–11]. Moreover, until recently these studies were made in inversion layers of Si-MOS (metal-oxide-semiconductor) structures [1,2] in GaAs/Al_xGa_{1-x}As selectively doped heterojunctions with two-subband occupied [3–5], where large-scale fluctuations of layers have small effect on the position of the energy levels and transport properties. Recently, new types of quantum wells (QW), e.g., modulation-doped QW [7], wide parabolic QW [8,9,11], and stepped QW [10] semiconductor structures with two occupied subbands, have been grown by tailoring the conduction-band edge of III-IV semiconductors. It was shown that these novel heterostructures with double subband occupancy exhibit a much stronger effect of large-scale disorder on transport properties than the previously studied one-subband systems. For the new systems, the screening is effective only on the average of the external changes of the bottoms of the two occupied subbands, which are different from each other, and caused by smooth variations of QW parameters on the scale of the Bohr radius as illustrated in Fig. 1a. Only essential unscreened large-scale fluctuations of the both occupied QW levels are present in these systems.

This paper addresses the effect of such non-screened variations of both occupied energy levels on the electronic spectrum and the classical magnetotransport by employing different confinement models: hard wall QW (Fig. 1b), parabolic QW (Fig. 1c), and stepped QW (Fig. 1d). Short-range and small-angle elastic scattering mechanisms, within a local response approximation, are included in the linearized kinetic equation. We obtain effective magnetotransport coefficients, which are evaluated from the components of the local conductivity tensor averaged over large-scale inhomogeneities, up to second order in the disorder contributions to the conductivity [12], for zero temperature. In addition, we calculate the modulation of the effective conductivity by the transverse voltage. We take into account the difference between intra-subband momentum scattering frequencies and the inter-subband contributions. We investigate also the spatial variations of these frequencies. We find an essential broadening of the peak of intersubband transitions due to the large-scale inhomogeneities and we provide numerical estimates of magnetotransport coefficients for the considered models.

The organization of the paper is as follows. In Sec. II the energy spectrum, which takes into account non-screened variations of levels, and the general conductivity tensor within the linear response approach, are obtained. From the transition probability for a random potential model, we calculate, in Sec. III, the scattering frequencies and magnetotransport coefficients considering short-range and small-angle scattering mechanisms and after averaging the conductivity tensor over in-plane large-scale inhomogeneities. In Sec. IV, we discuss the assumptions, on which the work described here is explicitly dependent, and we present our concluding remarks.

II. GENERAL EQUATIONS

We discuss now our model for the energy levels fluctuations due to random inhomogeneities and we obtain the general expressions of the conductivity tensor based on the local response approach for nonideal QWs with two occupied subbands.

A. Electron energy spectrum

Electron energy levels in a QW with slowly varying width can be described in terms of $\mathbf{r} = \{x, y\}$ along with the in-plane kinetic energy given by the parabolic dispersion law $\varepsilon_p = p^2/2m$ with effective mass m . For instance, the influence of nonideal heterointerfaces in the hard-wall QW, formed by large band offsets, can be studied by assuming that the QW widths, $d_{\mathbf{r}}$, are randomly varied. Then, the few lowest energy levels $s = 1, 2, \dots$ are given by

$$\varepsilon_{s\mathbf{r}} = \frac{(s\pi\hbar/d_{\mathbf{r}})^2}{2m} \simeq \varepsilon_s \left(1 - 2\frac{\delta d_{\mathbf{r}}}{d} \right), \quad (1)$$

where $\varepsilon_s = s^2(\pi\hbar/d)^2/2m$, d is the mean width of the QW, and $\delta d_{\mathbf{r}}$ is its random fluctuation due to heterointerface roughness. The energy of an electron in the s -th subband is given as $E_{p\mathbf{r}}^{(s)} = p^2/2m + \varepsilon_{s\mathbf{r}} + v_{s\mathbf{r}}$, where $v_{s\mathbf{r}} = \int dz |\varphi_{sz}|^2 V_{\mathbf{r}z}$ is the screening potential averaged over the s -th subband charge distribution $|\varphi_{sz}|^2$ along the z direction. The potential $V_{\mathbf{r}z}$ is determined by the Poisson's equation as

$$\nabla^2 V_{\mathbf{r}z} = -\frac{4\pi e^2}{\epsilon} (n_{\mathbf{r}z} - \langle n_{\mathbf{r}z} \rangle), \quad n_{\mathbf{r}z} = \sum_{s=1,2} n_{s\mathbf{r}} |\varphi_{sz}|^2, \quad (2)$$

where $n_{s\mathbf{r}} = \rho_{2D}(\varepsilon_F - \varepsilon_{s\mathbf{r}} - v_{s\mathbf{r}})$ is the electron density in the s -th subband, $\rho_{2D} = m/\pi\hbar^2$ is the 2D density of states, ε_F the Fermi energy, $\langle n_{\mathbf{r}z} \rangle$ is the electron density averaged over the random inhomogeneities, and ϵ is the dielectric constant, assumed independent of z . Hereafter, we consider only the case of two occupied subbands.

The solution of Eq. (2) is given as

$$V_{\mathbf{q}z} = \frac{2\pi e^2}{\epsilon q} \int dz' e^{-q|z-z'|} \delta n_{\mathbf{q}z'}, \quad (3)$$

where $\delta n_{\mathbf{q}z}$ is the 2D Fourier transform of the nonuniform part of the electron density

$$\delta n_{\mathbf{r}z} = \sum_{s=1,2} |\varphi_{sz}|^2 \delta n_{s\mathbf{r}} = -\rho_{2D} \sum_s |\varphi_{sz}|^2 (\delta \varepsilon_{s\mathbf{r}} + v_{s\mathbf{r}}). \quad (4)$$

Substituting Eq. (4) in Eq. (3), we are led to the system of two linear inhomogeneous equations for the Fourier transforms of screening potentials $v_{s\mathbf{q}}$ for $s = 1$ and $s = 2$ subbands:

$$v_{s\mathbf{q}} = -\frac{2\pi e^2}{\epsilon q} \rho_{2D} \sum_{s'} \int dz \varphi_{sz}^2 \int dz' e^{-q|z-z'|} |\varphi_{s'z'}|^2 (\delta \varepsilon_{s'\mathbf{q}} + v_{s'\mathbf{q}}). \quad (5)$$

Notice that inhomogeneity of Eq. (5) comes from terms $\propto \delta \varepsilon_{s'\mathbf{q}}$. Hence the solutions are expressed in terms of the variations of the occupied levels, introduced by Eq. (1). Assuming large-scale variations, $\ell_c \gg d$, it follows from Eq. (5) that only the Fourier components with $q \lesssim \ell_c^{-1} \ll d^{-1}$ are essential. Then $\exp(-q|z - z'|)$ in Eq. (5) can be well approximated by the unity and we have

$$v_{s\mathbf{q}} = -\frac{4}{qa_B} \sum_{s'} (\delta\varepsilon_{s'\mathbf{q}} + v_{s'\mathbf{q}}), \quad (6)$$

where a_B is the Bohr radius. Here the right-hand side is independent of s , so $v_{1,2\mathbf{q}} \equiv v_{\mathbf{q}}$. Further, for $qa_B/8 \ll 1$, from Eq. (6), it follows that

$$v_{\mathbf{r}} \simeq -\frac{1}{2} \sum_{s=1,2} \delta\varepsilon_{s\mathbf{r}}, \quad (7)$$

i.e., screening is relevant only on the average of the external variations $\delta\varepsilon_{1\mathbf{r}}$ and $\delta\varepsilon_{2\mathbf{r}}$. As a result, the electron spectrum energy can be written in the form

$$E_{p\mathbf{r}}^{(s)} = \frac{p^2}{2m} + \varepsilon_s - (-1)^s \delta\varepsilon_{\mathbf{r}}, \quad (8)$$

where $\delta\varepsilon_{\mathbf{r}} = (\varepsilon_2 - \varepsilon_1)\delta d_{\mathbf{r}}/d \approx 3\varepsilon_1\delta d_{\mathbf{r}}/d$ is the non-screened part of potential. For further numerical estimates, we assume Gaussian correlations for the QW width fluctuations

$$\langle \delta\varepsilon_{\mathbf{r}} \delta\varepsilon_{\mathbf{r}'} \rangle = \left(\frac{3\varepsilon_1}{d} \right)^2 \langle \delta d_{\mathbf{r}} \delta d_{\mathbf{r}'} \rangle = (\overline{\delta\varepsilon})^2 w(|\mathbf{r} - \mathbf{r}'|). \quad (9)$$

Here $\overline{\delta\varepsilon} = 3\varepsilon_1\overline{\delta d}/d$, $\overline{\delta d}$ is the typical height of the roughness interface and $w(x) = \exp[-(x/\ell)^2]$ is the Gaussian function with lateral correlation length ℓ . We can also write analogous expressions for the case of parabolic (Fig. 1c) and stepped (Fig. 1d) QWs but we do not give here the pertinent formulas considering further that $\overline{\delta\varepsilon}$ is a given quantity.

B. Conductivity tensor

Classical transport phenomena for electrons with spectrum, given by Eq. (8), are described by the distribution function $f_F(E_{p\mathbf{r}}^{(s)}) + \Delta f_{p\mathbf{r}}^{(s)}$ within the linear response theory. Here f_F is the unperturbed Fermi distribution and the field-induced distribution is determined from the linearized kinetic equation of s -th subband given by

$$\left(\mathbf{v} \cdot \nabla_{\mathbf{r}} + (-1)^s \nabla \delta\varepsilon_{\mathbf{r}} \cdot \frac{\partial}{\partial \mathbf{p}} + \frac{e}{c} [\mathbf{v} \times \mathbf{H}] \cdot \frac{\partial}{\partial \mathbf{p}} \right) \Delta f_{p\mathbf{r}}^{(s)} - I_s(\Delta f | \mathbf{p}\mathbf{r}) = -e \mathbf{E}_{\mathbf{r}} \cdot \frac{\partial f_F(E_{p\mathbf{r}}^{(s)})}{\partial \mathbf{p}}, \quad (10)$$

where $\mathbf{E}_{\mathbf{r}}$ is the electric field, which is zero in the absence of a net current density $\mathbf{j}_{\mathbf{r}}$, \mathbf{H} is the magnetic field perpendicular to the QW's plane ($\mathbf{v} = \mathbf{p}/m$) and the collision integral for the elastic scattering case is written as

$$I_s(\Delta f | \mathbf{p}\mathbf{r}) = \sum_{s' \mathbf{p}'} W_{\mathbf{p}\mathbf{p}'}^{ss'} (\Delta f_{\mathbf{p}'\mathbf{r}}^{(s')} - \Delta f_{\mathbf{p}\mathbf{r}}^{(s)}). \quad (11)$$

$W_{\mathbf{p}\mathbf{p}'}^{ss'}$ is the transition probability per second between states s, \mathbf{p} and s', \mathbf{p}' . The total current density $\mathbf{j}_{\mathbf{r}}$ is given by the standard expression $\mathbf{j}_{\mathbf{r}} = (2e/L^2) \sum_{s\mathbf{p}} \mathbf{v} \Delta f_{\mathbf{p}\mathbf{r}}^{(s)}$ and satisfies the continuity equation $\nabla \cdot \mathbf{j}_{\mathbf{r}} = 0$.

The contributions from the convection and random fields in the left-hand side of Eq. (10) are estimated as \bar{v}/ℓ and $\overline{\delta\varepsilon}/(\bar{p}\ell)$ respectively. These contributions can be discarded when $\bar{v}\bar{\tau} \ll \ell$ and $\overline{\delta\varepsilon} \ll \bar{e}$, where $\bar{e} = \bar{v}\bar{p}/2$ is the characteristics electron energy, where we have used the relaxation time approximation to estimate the collision integral as $\bar{\tau}^{-1}$. Under these assumptions, Eq. (10) assumes the form

$$\frac{e}{c} [\mathbf{v} \times \mathbf{H}] \frac{\partial}{\partial \mathbf{p}} \Delta f_{p\mathbf{r}}^{(s)} - I_s(\Delta f | \mathbf{p}\mathbf{r}) = -e (\mathbf{E}_{\mathbf{r}} \cdot \mathbf{v}) f'_F(E_{p\mathbf{r}}^{(s)}), \quad (12)$$

where $f'_F(E) = \partial f_F(E)/\partial E$. We look for a solution in the form

$$\Delta f_{p\mathbf{r}}^{(s)} = -e f'_F(E_{p\mathbf{r}}^{(s)}) \left\{ A_s (\mathbf{E}_{\mathbf{r}} \cdot \mathbf{v}) + B_s \frac{e}{mc} ([\mathbf{E}_{\mathbf{r}} \times \mathbf{H}] \cdot \mathbf{v}) \right\}, \quad (13)$$

where the coefficients A_s and B_s depend only on p^2 . Substituting Eq. (13) into the kinetic equation (12), we obtain the linear algebraic system (see Ref. [11] for details)

$$\begin{aligned} \omega_c^2 B_s - \sum_{s' \mathbf{p}'} W_{\mathbf{p} \mathbf{p}'}^{ss'} \left(A_{s'} \frac{p'}{p} \cos(\mathbf{p}, \mathbf{p}') - A_s \right) &= 1, \\ A_s + \sum_{s' \mathbf{p}'} W_{\mathbf{p} \mathbf{p}'}^{ss'} \left(B_{s'} \frac{p'}{p} \cos(\mathbf{p}, \mathbf{p}') - B_s \right) &= 0. \end{aligned} \quad (14)$$

The solution of Eq. (14) for our two-level system is expressed through the transport relaxation frequency of s -th subband given by

$$\nu_s^{tr} = \sum_{\mathbf{p}'} W_{\mathbf{p} \mathbf{p}'}^{ss} [1 - \cos(\mathbf{p}, \mathbf{p}')] \quad (15)$$

and the intersubband relaxation frequencies are written as

$$\nu_{ss'} = \sum_{\mathbf{p}'} W_{\mathbf{p} \mathbf{p}'}^{ss'}, \quad \tilde{\nu}_{ss'} = \sum_{\mathbf{p}'} W_{\mathbf{p} \mathbf{p}'}^{ss'} \cos(\mathbf{p}, \mathbf{p}'), \quad (16)$$

where $s, s' = 1, 2$. The solution of Eqs. (14) is

$$\begin{aligned} A_1 &= \frac{\nu_1 [\omega_c^2 + \nu_2^2 + \eta_1 \tilde{\nu}_{12} \nu_2] - \tilde{\nu}_{12} [\tilde{\nu}_{12} \nu_2 + \eta_1 (\omega_c^2 + \tilde{\nu}_{12}^2)]}{\Delta} \\ B_1 &= \frac{\omega_c^2 + \nu_2^2 + \tilde{\nu}_{12}^2 + \eta_1 \tilde{\nu}_{12} (\nu_1 + \nu_2)}{\Delta}, \end{aligned} \quad (17)$$

with the cyclotron frequency $\omega_c = |e|H/mc$, $\nu_1 = \nu_1^{tr} + \nu_{12}$, $\nu_2 = \nu_2^{tr} + \nu_{12}$, and $\Delta = [(\nu_1 \nu_2 - \tilde{\nu}_{12}^2)^2 + \omega_c^2 (\omega_c^2 + \nu_1^2 + \nu_2^2 + 2\tilde{\nu}_{12}^2)]$. In Eq. (17) we have $\eta_1 = p'/p$, where the momenta p' and p are connected through $(p^2 - p'^2)/(2m) = \varepsilon_2 - \varepsilon_1 - 2\delta\varepsilon_{\mathbf{r}}$ from energy conservation. The expressions for A_2 and B_2 follows from the above expressions for A_1 and B_1 , respectively, by changing $1 \rightarrow 2$, $2 \rightarrow 1$ everywhere in Eq. (17) and taking $\eta_2 = p'/p$ where p' now satisfies $(p^2 - p'^2)/(2m) = \varepsilon_1 - \varepsilon_2 + 2\delta\varepsilon_{\mathbf{r}}$.

Furthermore, for the zero-temperature, the coefficients A_s and B_s are calculated only at the Fermi level. Thus, we have to use $p = p_{F_1}$ ($p = p_{F_2}$) in A_1, B_1 (A_2, B_2) while $\eta_1 = p_{F_2}/p_{F_1}$ and $\eta_2 = p_{F_1}/p_{F_2}$ correspondingly. The induced current density, at zero temperature, is written as

$$\mathbf{j}_{\mathbf{r}} = \frac{e^2}{m} \sum_s n_{\mathbf{r}}^{(s)} \left\{ A_s \mathbf{E}_{\mathbf{r}} + B_s \frac{e}{mc} [\mathbf{E}_{\mathbf{r}} \times \mathbf{H}] \right\} \equiv \hat{\sigma}(\mathbf{r}) \mathbf{E}_{\mathbf{r}}, \quad (18)$$

where the electron concentration for the s -th subband is given by

$$n_{\mathbf{r}}^{(s)} = n_s + (-1)^s \rho_{2D} \delta\varepsilon_{\mathbf{r}}. \quad (19)$$

n_s is the mean concentration of the s -th level and $n = n_1 + n_2$ is the total average concentration. From Eq. (18), the components of the 2×2 conductivity tensor are

$$\sigma_{xx}(\mathbf{r}) = \frac{e^2}{m} \sum_s A_s n_{\mathbf{r}}^{(s)}, \quad \sigma_{yx}(\mathbf{r}) = \frac{e^2}{m} \omega_c \sum_s B_s n_{\mathbf{r}}^{(s)}, \quad (20)$$

where $\sigma_{xx}(\mathbf{r}) = \sigma_{yy}(\mathbf{r})$ and $\sigma_{yx}(\mathbf{r}) = -\sigma_{xy}(\mathbf{r})$. Note, that the conductivity dependence on \mathbf{r} comes not only due to the spatial variations of $n_{\mathbf{r}}^{(s)}$ but also because p_{F_1} and p_{F_2} depends on \mathbf{r} .

III. TRANSPORT PROPERTIES

In this section, we study the peculiarities of the steady-state magnetotransport caused by unscreened fluctuations of the QW's energy levels. In the model of random potentials, the transition probability can be written as

$$W_{\mathbf{p} \mathbf{p}'}^{ss'} = \frac{2\pi w}{\hbar L^3} \sum_q \exp[-(Q/q_0)^2] |\langle s' | e^{iqz} | s \rangle|^2 \delta(E_{\mathbf{p}', s', \mathbf{r}} - E_{\mathbf{p}, s, \mathbf{r}}), \quad (21)$$

where $w \exp(-Q^2/q_0^2)$ is the Gaussian correlation function for the random potential with characteristic scale q_0^{-1} (note that $q_0 \gg \ell^{-1}$), $\mathbf{Q} = [(\mathbf{p}' - \mathbf{p})/\hbar, q]$ is a 3D wave vector, and L is the normalization length. Summing over q in Eq. (21) leads to

$$K_{ss'} = \frac{1}{L} \sum_q e^{-(q/q_0)^2} |\langle s' | e^{iqz} | s \rangle|^2 = \frac{q_0}{2\sqrt{\pi}} \int dz \int dz' \varphi_{s'z} \varphi_{sz} \varphi_{s'z'} \varphi_{sz'} e^{-[q_0(z-z')/2]^2} \quad (22)$$

and the transition probability transforms into

$$W_{\mathbf{pp}'}^{ss'} = \frac{2\pi w}{\hbar L^2} \exp\{-(\mathbf{p}' - \mathbf{p})/\hbar q_0\}^2 K_{ss'} \delta(E_{\mathbf{p}',s',\mathbf{r}} - E_{\mathbf{p},s,\mathbf{r}}), \quad (23)$$

where the δ -function depends on \mathbf{r} only for intersubband transitions, $s \neq s'$. Notice that $K_{12} = K_{21}$.

The functions $K_{ss'}$ are calculated below for the cases of short-range ($q_0^{-1} \ll d$) and small-angle ($\hbar q_0 \ll p_{Fs}$) scattering. We consider three models of confinement potential: hard-wall QWs (see Sec. IIA), parabolic QWs [8,9] with effective width $\ell_\perp = \sqrt{\hbar/m\omega_\perp}$, ω_\perp is the characteristic frequency of the potential, and stepped QWs [10] with quite different well widths $d_n \ll d_w$. The coefficients $K_{ss'}$ are shown in Table I.

Consider next the relaxation frequencies for these cases. For short-range scattering, straightforward calculations of Eqs. (15), (16), and (23) give

$$\nu_1^{tr} = (mw/\hbar^3)K_{11}, \quad \nu_2^{tr} = (mw/\hbar^3)K_{22}, \quad \nu_{12} = (mw/\hbar^3)K_{12}, \quad (24)$$

and $\tilde{\nu}_{12} = 0$. For small-angle scattering, we obtain

$$\nu_{1,2}^{tr} \approx \frac{mwq_0^3}{8\sqrt{\pi}p_{F_{1,2}}^3} K_{11}, \quad \text{and} \quad \nu_{12} \approx \tilde{\nu}_{12} \approx \frac{mwq_0}{2\sqrt{\pi}\hbar^2\sqrt{p_{F_1}p_{F_2}}} K_{12} e^{-(p_{F_1}-p_{F_2})^2/\hbar^2q_0^2}, \quad (25)$$

where we assumed that $(\hbar q_0/p_{F_s})^2 \ll 1$ and p_{F_s} is determined from $E_{p\mathbf{r}}^{(s)} = E_F$. We point out that, in these conditions for small-angle scattering, we have $\nu_{12} \ll \nu_s^{tr}$ due to the exponentially small factor. Indeed, for instance, in the case of the parabolic QW, $\nu_{12}/\nu_1^{tr} = \sqrt{p_{F_1}/p_{F_2}}(p_{F_1}\ell_\perp/\hbar)^2 \exp[-(p_{F_1}-p_{F_2})^2/\hbar^2q_0^2]$. For the maximum ratio p_{F_1}/p_{F_2} , we estimate $\nu_{12}/\nu_1^{tr} = 4\sqrt{2} \exp[-(p_{F_1}-p_{F_2})^2/\hbar^2q_0^2]$. So, if $\exp[-(p_{F_1}-p_{F_2})^2/\hbar^2q_0^2] \ll 10^{-1}$, we obtain $\nu_{12}/\nu_s^{tr} \ll 1$ for hard-wall and parabolic QWs. Similar condition holds for the stepped QW. For small-angle scattering, we neglect further very small contributions related to $\tilde{\nu}_{12}$ and ν_{12} . Then, as it is seen in the Table I and Eq. (25), the transport coefficients do not depend essentially on the specific QW for small-angle scattering.

In order to analyze the influence of non-uniform contributions, we have to average the local conductivity tensor, Eqs. (20), written in the form $\sigma_{\mu\nu}(\mathbf{r}) = \langle \sigma_{\mu\nu} \rangle + \sum_{\mathbf{k}} (\delta\sigma_{\mathbf{k}})_{\mu\nu} \exp(i\mathbf{k} \cdot \mathbf{r})$, where $\delta\sigma_{\mathbf{k}}$ is the non-uniform contribution and $\langle \sigma_{\mu\nu} \rangle$ is the conductivity tensor for an ideal QW with two occupied subbands given by

$$\langle \sigma_{\mu\nu} \rangle = \frac{e^2}{m} \sum_s \frac{n_s}{\nu_s^2 + \omega_c^2} \begin{cases} \nu_s & \mu = x, \nu = x, \\ \omega_c & \mu = y, \nu = x \end{cases}. \quad (26)$$

Here we assume that intersubband frequencies are negligible. Following Ref. [12], we obtain, up to the second order in the large-scale disorder, the effective conductivity tensor, from $\langle \mathbf{j}_\mathbf{r} \rangle = \hat{\sigma}^{eff} \langle \mathbf{E}_\mathbf{r} \rangle$, as

$$\sigma_{\mu\nu}^{eff} = \langle \sigma_{\mu\nu} \rangle - \sum_{\mathbf{k}} \frac{\sum_{\alpha\beta} \langle (\delta\sigma_{-\mathbf{k}})_{\mu\alpha} k_\alpha k_\beta (\delta\sigma_{\mathbf{k}})_{\beta\nu} \rangle}{\sum_{\alpha\beta} k_\alpha \sigma_{\alpha\beta} k_\beta}, \quad (27)$$

where $\langle \dots \rangle$ denotes the average over the sample area, *i.e.*, for distances $r \gg \ell$, and $\langle \sum_{\mathbf{k}} (\delta\sigma_{\mathbf{k}})_{\mu\nu} \exp(i\mathbf{k} \cdot \mathbf{r}) \rangle = 0$ [12]. The average is performed using Fourier transform of the Gaussian correlation function, Eq. (9), $\langle \delta\varepsilon_{\mathbf{k}} \delta\varepsilon_{\mathbf{k}'} \rangle = \delta_{\mathbf{k}+\mathbf{k}',0} (\pi \overline{\delta\varepsilon^2} \ell_c^2 / L^2) \exp[-(k\ell_c/2)^2]$ with $k = \sqrt{k_x^2 + k_y^2}$.

A. Short-range scattering

Before explicit calculation of the local magnetoconductivity tensor from the general Eq. (20), we present now standard expressions for magnetotransport coefficients of a QW with two occupied subbands. Using the conductivity tensor, given by Eq. (26), we obtain the magnetoresistance

$$\Delta\rho_{\perp} = \frac{n_1 n_2 \omega_c^2 (\nu_1 - \nu_2)^2}{\nu_1 \nu_2 [(n_1 + n_2)^2 \omega_c^2 + (n_1 \nu_2 + n_2 \nu_1)^2]}, \quad (28)$$

and the Hall coefficient

$$R = \frac{1}{ec} \frac{n_1 (\nu_2^2 + \omega_c^2) + n_2 (\nu_1^2 + \omega_c^2)}{[n_1^2 (\nu_2^2 + \omega_c^2) + n_2^2 (\nu_1^2 + \omega_c^2) + 2n_1 n_2 (\nu_2 \nu_1 + \omega_c^2)]}. \quad (29)$$

For strong ($\omega_c \tau \gg 1$) and weak ($\omega_c \tau \ll 1$) magnetic fields, the Hall coefficient do not depend on H leading to $R(\infty) \approx 1/ec(n_1 + n_2)$ and $R(H = 0) \approx (n_1 \nu_2^2 + n_2 \nu_1^2) / [ec(n_1 \nu_2 + n_2 \nu_1)^2]$.

For short-range scattering, all frequencies do not depend on $p_{F_{1,2}}$ and as a consequence, the coefficients A_s and B_s are independent of \mathbf{r} . The non-uniform contribution to the conductivity tensor takes the form

$$\delta\sigma_{\mu\nu}(\mathbf{k}) = \frac{e^2 \rho_{2D}}{m} \sum_s \frac{(-1)^s \delta\varepsilon_{\mathbf{k}}}{\nu_s^2 + \omega_c^2} \begin{cases} \nu_s & \mu = x, y \quad \nu = x, y \\ \omega_c & \mu = y, \quad \nu = x \end{cases}. \quad (30)$$

After substituting Eq. (30) into Eq. (27) and performing the averaging process, we obtain the components of the effective conductivity tensor as

$$\sigma_{xx}^{eff} = \langle \sigma_{xx} \rangle - \frac{e^4 \overline{\delta n}^2}{2m^2 \langle \sigma_{xx} \rangle} \left(\frac{1}{\omega_c^2 + \nu_1^2} + \frac{1}{\omega_c^2 + \nu_2^2} - \frac{2(\omega_c^2 + \nu_1 \nu_2)}{(\omega_c^2 + \nu_1 \nu_2)^2 + \omega_c^2(\nu_2 - \nu_1)^2} \right), \quad (31)$$

$$\sigma_{yx}^{eff} = \langle \sigma_{yx} \rangle - \frac{e^4 \overline{\delta n}^2}{m^2 \langle \sigma_{xx} \rangle} \omega_c \left(\frac{1}{\omega_c^2 + \nu_1^2} - \frac{1}{\omega_c^2 + \nu_2^2} \right) \left(\frac{\nu_1}{\omega_c^2 + \nu_1^2} - \frac{\nu_2}{\omega_c^2 + \nu_2^2} \right), \quad (32)$$

where $\overline{\delta n} = \rho_{2D} \overline{\delta\varepsilon}$ gives the concentration fluctuation due to large-scale inhomogeneities.

Using Eqs. (31) and (32), the effective magnetoresistance $\Delta\rho_{eff}$, and the Hall coefficient R_{eff} , can be easily obtained. In Fig. 2, we plot $\Delta\rho_{eff}$ as a function of the magnetic field for $n_2/n_1 = 0.5$. The solid and dot-dashed curves are 10 times enlarged and correspond to parabolic QWs where $\nu_2/\nu_1 = 5/6$ and $\overline{\delta n}/n_1 = 0.2$ and $\overline{\delta n}/n_1 = 0$ respectively, The dotted and dashed curves correspond to stepped QWs for $\overline{\delta n}/n_1 = 0.2$ and $\overline{\delta n}/n_1 = 0$, respectively, with $d_n \approx 10 \text{ \AA}$, $d_w \approx 350 \text{ \AA}$, $U_0 \approx 0.1 \text{ eV}$, which leads to $\kappa \approx 10^6 \text{ cm}^{-1}$, $\varepsilon_2 - \varepsilon_1 \approx 21.5 \text{ meV}$, and $n_1 + n_2 \approx 2.0 \times 10^{12} \text{ cm}^{-2}$. It follows that $\nu_2/\nu_1 = 1/2.1$. Notice that $\Delta\rho_{eff} \equiv 0$ as well as $\Delta\rho_{\perp} \equiv 0$ for the hard-wall QW because $\nu_2/\nu_1 = 1$ for short-range scattering. Then magnetoresistance is absent for hard-wall QWs, while a positive magnetoresistance appears for the parabolic QW, which becomes larger by a factor of 15 in the case of the stepped QW.

In Fig. 3, we depict $(R_{eff} - R_0)/R_0$, where $R_0 = 1/ecn$ with $n = (n_1 + n_2)$ using the same curves and conditions as in Fig. 2. Similarly to Fig. 2, the solid and dot-dashed curves represent $10 \times (R_{eff} - R_0)/R_0$ for the parabolic QW. In the case of the hard-wall QW, $R_{eff} \equiv R_0$ and $R \equiv R_0$ because $\nu_2/\nu_1 = 1$. Hence for hard-wall QW $(R_{eff} - R_0)/R_0 = 0$, while an explicit dependence of H is observed for parabolic and stepped QWs. In addition, from Figs. 2,3 it follows that unscreened effect of the large-scale inhomogeneities of a QW parameters is manifested through stronger magnetoresistance at $\omega_c/\nu_1 < 1$ and weaker at $\omega_c/\nu_1 > 1$. While it leads to smaller Hall coefficient for $\omega_c/\nu_1 < 0.5$, for $\omega_c/\nu_1 \gtrsim 2$ effect of such large-scale inhomogeneities on Hall coefficient becomes negligible. Notice that in experiment of Ref. [8] it was observed for magnetic fields, $B_z < 0.2 \text{ T}$, practically independent of H_z magnetoresistance in GaAs-based parabolic QW with two occupied subbands: which leads to ν_1 very close to ν_2 that in turn can be valid only when scattering is short-range.

B. Small-angle scattering

For small-angle scattering, large-scale fluctuations of the electron density and scattering frequencies play an important role. As we have seen, scattering frequencies, given by Eq. (25), depend on fluctuations of the Fermi momenta. Further, we can neglect contributions coming from ν_{12} and $\tilde{\nu}_{12}$. Using Eqs. (17), (20), (25), and (27), the components of the effective conductivity tensor, for small-angle scattering, can be written as

$$\sigma_{xx}^{eff} / \overline{\sigma}_0 = \overline{\sigma}_{xx} - \frac{4 \overline{\delta n}^2}{n^2 \overline{\sigma}_{xx}} [F_x^2(H) - F_y^2(H)], \quad (33)$$

and

$$\sigma_{yx}^{eff}/\bar{\sigma}_0 = \bar{\sigma}_{yx} - \frac{8\bar{\delta n}^2}{n^2\bar{\sigma}_{xx}} F_y(H) F_x(H), \quad (34)$$

where

$$\bar{\sigma}_{xx} = \langle \sigma_{xx} \rangle / \bar{\sigma}_0 = 2\sqrt{2} \sum_{s=1,2} \frac{(n_s/n_{2D})^{1/2}}{1 + \omega_c^2/\nu_s^2} \left\{ \left(\frac{n_s}{n} \right)^2 + \frac{\bar{\delta n}^2}{n^2} \left[-\frac{19}{16} + \left(\frac{7}{4} - \frac{3\omega_c^2/\nu_s^2}{1 + \omega_c^2/\nu_s^2} \right)^2 \right] \right\}, \quad (35)$$

$$\bar{\sigma}_{yx} = \langle \sigma_{yx} \rangle / \bar{\sigma}_0 = 2\sqrt{2} \sum_{s=1,2} \frac{(\omega_c/\nu_s)(n_s/n)^{1/2}}{1 + \omega_c^2/\nu_s^2} \left\{ \left(\frac{n_s}{n} \right)^2 + \frac{\bar{\delta n}^2}{n^2} \left[-\frac{1}{4} + \left(\frac{5}{2} - \frac{3\omega_c^2/\nu_s^2}{1 + \omega_c^2/\nu_s^2} \right)^2 \right] \right\}, \quad (36)$$

and

$$F_x(H) = \sum_{s=1,2} (-1)^s \frac{(n_s/n)^{3/2}}{1 + \omega_c^2/\nu_s^2} \left(\frac{5}{2} - \frac{3\omega_c^2/\nu_s^2}{1 + \omega_c^2/\nu_s^2} \right), \quad (37)$$

$$F_y(H) = \sum_{s=1,2} (-1)^s \frac{(\omega_c/\nu_s)(n_s/n)^{3/2}}{1 + \omega_c^2/\nu_s^2} \left(4 - \frac{3\omega_c^2/\nu_s^2}{1 + \omega_c^2/\nu_s^2} \right). \quad (38)$$

Here $\nu_s = mwq_0^4/16\pi\bar{p}_{F_s}^3$, where \bar{p}_{F_s} is independent of \mathbf{r} and is determined by n_s , $\bar{\sigma}_0 = e^2n/m\nu_0$, and a typical scattering frequency ν_0 is determined as $\nu_0^{-2/3} = (\nu_1^{-2/3} + \nu_2^{-2/3})/2$. Notice that ν_s is related to n_s , while ν_0 corresponds to $n/2$. In Figs. 4 and 5 we present our calculated effective conductivity tensor, given by Eqs. (33)-(38), magnetoresistance $\Delta\rho_{eff}$ and the Hall coefficient, R_{eff} .

In Fig. 4, we show $\Delta\rho_{eff}$ for $n_2/n_1 = 0.5$ as a function of ω_c/ν_1 . The solid and dashed curves represent $\Delta\rho_{eff}$ for small-angle scattering for $\bar{\delta n}/n = 1/8$ and $\bar{\delta n}/n = 0$, respectively, and $\nu_2/\nu_1 = 8$. For comparison, we plot the dotted curve for short-range scattering in the stepped QW as shown in Fig. 2. We observe in Fig. 4 that, for small-angle scattering, large-scale inhomogeneities strongly modifies the effective magnetoresistance in the case of two occupied subbands. Its behavior can be essentially different from the situation of short-range scattering. In this case, as it can be seen in Fig. 2, the magnetoresistance increases before reaching a plateau at $\omega_c/\nu_1 \gtrsim 1$. On the contrary, for small-angle scattering, this behavior is observed at $\omega_c/\nu_1 \gtrsim 8$. As it is seen in Fig. 4, there is a much larger region of classical magnetic fields in which the magnetoresistance increases in case of small-angle scattering than for short-range scattering. Furthermore, in contrast with the short-range scattering case, we see that large-scale unscreened inhomogeneities lead to substantially smaller values of magnetoresistance at relatively weak magnetic fields, $\omega_c/\nu_1 \lesssim 3$, while contributes to enhance the magnetoresistance at larger magnetic fields, $\omega_c/\nu_1 \gtrsim 4$. Notice that according experimental results of Ref. [11], where all data are given for $n_2/n_1 \approx 1/2$, the rather small magnetoresistance was attributed to small-angle scattering, which is confirmed by our calculated $\Delta\rho_{eff}$ given by the solid curve in Fig. 4.

Using the same parameters of Fig. 4, $(R_{eff} - R_0)/R_0$ is depicted in Fig. 5. We now observe that large-scale unscreened inhomogeneities lead to a substantially weaker dependence of R_{eff} on H in agreement with the experimental results of Ref. [11]. In conclusion, our theoretical results describe qualitatively well the experimental ones. [11] We point out that the results, in the case of small-angle scattering, are independent of QW confinement model.

C. Transverse field effect on the conductivity

Now we consider the modulation of the effective conductivity under transverse voltage which causes intersubband redistribution of the electron population. From Eq. (31), for zero magnetic field, the effective conductivity, for short-range scattering, can be written as

$$\sigma^{eff}/\bar{\sigma} = \left(1 + \frac{\Delta n \Delta \nu}{n \bar{\nu}} \right) \left\{ 1 - 2 \frac{\bar{\delta n}^2 \Delta \nu^2}{n^2 \bar{\nu}^2 (1 + \Delta n \Delta \nu / n \bar{\nu})^2} \right\}, \quad (39)$$

where $\bar{\sigma} = e^2 n \bar{\nu} / m \nu_1 \nu_2$, $\bar{\nu} = (\nu_1 + \nu_2) / 2$, $\Delta\nu = (\nu_2 - \nu_1) / 2$, $\Delta n = (n_1 - n_2) = \rho_{2D}(\varepsilon_2 - \varepsilon_1)$ with $n_1 = (n + \Delta n) / 2$ and $n_2 = (n - \Delta n) / 2$. For hard-wall QWs, because $\Delta\nu = 0$, it follows that σ^{eff} is independent of Δn . In Fig. 6, we present $\Delta\sigma^{eff} = \sigma^{eff}/\bar{\sigma} - 1$ as a function of $\Delta n/n$. The dotted and dashed curves correspond to stepped QWs with $\Delta\nu/\bar{\nu} \approx -0.36$, for the same parameters used in Fig. 2, and $\bar{\delta}n/n = 1/8$ and $\bar{\delta}n/n = 0$, respectively. The thin-solid curve corresponds to a parabolic QW, with $\Delta\nu/\bar{\nu} = -1/11$, for $\bar{\delta}n/n = 1/8$ which practically coincides with that for $\bar{\delta}n/n = 0$. We observe that all curves, plotted in Fig. 6, for short-range scattering, have a negative slope.

For small-angle scattering, the effective conductivity, given by Eq. (33), transforms, for $H = 0$, into

$$\begin{aligned} \sigma^{eff}/\bar{\sigma}_0 &= \frac{1}{2} \left\{ \left(1 + \frac{\Delta n}{n}\right)^{5/2} + \left(1 - \frac{\Delta n}{n}\right)^{5/2} + \frac{15\bar{\delta}n^2}{2n^2} \left[\left(1 + \frac{\Delta n}{n}\right)^{1/2} + \left(1 - \frac{\Delta n}{n}\right)^{1/2} \right] \right\} \\ * &\times \left(1 - \frac{25\bar{\delta}n^2}{2n^2} \frac{\left[\left(1 + \frac{\Delta n}{n}\right)^{3/2} - \left(1 - \frac{\Delta n}{n}\right)^{3/2} \right]^2}{\left\{ \left(1 + \frac{\Delta n}{n}\right)^{5/2} + \left(1 - \frac{\Delta n}{n}\right)^{5/2} + \frac{15\bar{\delta}n^2}{2n^2} \left[\left(1 + \frac{\Delta n}{n}\right)^{1/2} + \left(1 - \frac{\Delta n}{n}\right)^{1/2} \right] \right\}^2} \right). \end{aligned} \quad (40)$$

In Fig. 6, we show the results of $\Delta\sigma^{eff} = \sigma^{eff}/\bar{\sigma}_0 - 1$ as a function of $\Delta n/n$, calculated from Eq. (40) and represented by solid and dot-dot-dashed curves, which correspond to $\bar{\delta}n/n = 1/8$ and $\bar{\delta}n/n = 0$, respectively. We see that in contrast with the short-range scattering, now the curves have a positive slope. We do not discuss here the relation between $\Delta n/n$ and the applied voltage. According to, for instance Refs. [9], [11] and electro-optical measurements (for references see Ref. [14]), the population redistribution can be essential already for rather small voltages. More detailed behavior can be achieved by performing self-consistent calculations for band structures with diagrams shown in Figs. 1(b-d).

IV. CONCLUDING REMARKS

We have shown that non-screened variations of the intersubband energy modify essentially the transport properties of quantum wells when two subbands are occupied. Relative changes in the transport coefficients are determined by the degree of the random redistribution of the electron density and by the extent of the asymmetry of scattering processes that, for short-range scattering, are characterized by dimensionless parameters $\bar{\delta}n/n$ and $\Delta\nu/\bar{\nu}$, respectively. Our model is founded on some assumptions, which we discuss below, and more detailed numerical calculations, which take into account peculiarities of the band structure and scattering mechanisms, are necessary for a full description of the electron transport. However, our results demonstrate that the kinetic coefficients change when we move from single to double subband occupancy in samples of similar quality.

Along with magnetotransport characteristics (magnetoresistance, the Hall coefficient, etc.) and the field effect (modulation of effective conductivity by transverse voltage), other transport phenomena like Shubnikov-de Haas oscillations and cyclotron resonance are influenced by non-screened variations of subbands. For instance, essential broadening of the peak of intersubband transitions of a QW, due to unscreened large-scale inhomogeneities, [13] takes place also in the case of two occupied subbands. The effect of such inhomogeneities on intersubband optical transitions also requires special study.

We discuss now the model assumptions. We have used the approximation of smooth inhomogeneities in several points: *i*) dependence of QW energy levels upon the in-plane coordinate \mathbf{r} ; *ii*) we have assumed that characteristic scale of smooth inhomogeneities $\ell \gg a_B$, and the screened potential, given by Eq. (7), results only on the average of variations of the energy levels; *iii*) the condition that the transport scattering length $\bar{v}\bar{\tau} \ll \ell$ mainly determines the regime of applicability of the treatment; *iv*) the approximation of small amplitudes for smooth inhomogeneities, which leads to conditions $\bar{\delta}n/n_{1,2} \ll 1$, reduces quantitatively the effects, but it allows to use theory applied to weakly large-scale inhomogeneous media [12]. In addition, our calculations are based on simple QW spectra models instead of detailed self-consistent calculations of the band structure. However, we believe that the model assumptions, which are commonly used, do not change the overall behavior and numerical estimates of the magnetotransport coefficients. We hope our work can stimulate further experimental study of the transport properties of nonideal QWs with multisubband occupancy in order to verify the effects of large-scale, unscreened inhomogeneities.

ACKNOWLEDGMENTS

This work was supported by grants Nos. 95/0789-3 and 98/10192-2 from Fundação de Amparo à Pesquisa de São Paulo (FAPESP). O. G. B and N. S. are grateful to Conselho Nacional de Desenvolvimento Científico e Tecnológico

(CNPq) for research fellowship.

- [1] E. D. Siggia, P. C. Kwok, Phys. Rev. B **2**, 1024 (1970).
- [2] S. Mori, T. Ando, Phys. Rev. B **19**, 6433 (1979).
- [3] H. L. Stormer, A. C. Gossard, W. Wiegmann, Solid State Commun. **41**, 707 (1982).
- [4] H. van Houten, J. G. Williamson, and M. E. I. Broekaart, Phys. Rev. B **37**, 2756 (1988).
- [5] R. Fletcher, E. Zaremba, M. D'Iorio, C. T. Foxon, and J. J. Harris, Phys. Rev. B **41**, 10649 (1990); D. R. Leadley, R. Fletcher, R. J. Nicolas, F. Tao, C. T. Foxon, J. J. Harris, Phys. Rev B **46**, 12439 (1992).
- [6] G.-Q. Hai, N. Studart, and F. M. Peeters, Phys. Rev. B **52**, 8363 (1995); G.-Q. Hai, N. Studart, G. E. Marques, F. M. Peeters, P. M. Koenraad, Physica E **2**, 222 (1998).
- [7] V. Piazza, P. Casarini, S. De Franceschi, M. Lazzarino, F. Beltram, C. Jacoboni, A. Bosacchi, and S. Franchi, Phys. Rev. B **57**, 10017 (1998).
- [8] K. Ensslin, A. Wixforth, S. Sundaram, P. F. Hopkins, J. H. English, and A.C. Gossard, Phys. Rev. B **47**, 1366 (1993).
- [9] G. Salis, B. Graf, K. Ensslin, K. Campman, K. Maranowski and A.C. Gossard, Phys. Rev. Lett. **79**, 5106 (1997).
- [10] P. F. Yuh, K. L. Wang, J. Appl. Phys. **65**, 4377 (1989); V. Berger, Semicond Sci. Technol. **9**, 1493 (1994); H. Li, Z. Wang, J. Liang, B. Xu, J. Xu, Q. Gong, C. Jiang, F. Liu, and W. Zhou, J. Appl. Phys. **82**, 6107 (1997).
- [11] S. A. Studenikin, A. V. Chaplik, I. A. Papaev, G. Salis, K. Ensslin, K. Maranowski and A. C. Gossard, Semicond Sci. Technol. **14**, 604 (1999).
- [12] C. Herring, Journ. Appl. Phys. **31**, 1939 (1960).
- [13] F. T. Vasko, J. P. Sun, G. I. Haddad, and V. V. Mitin, J. Appl. Phys., April, (2000).
- [14] F. T. Vasko and A. Kuznetsov, *Electronic States and Optical Transitions in Semiconductor Heterostructures*, Springer-Verlag, Berlin (1998).

TABLE I. Coefficients $K_{ss'}$, which appear in the transition probability given by Eq. (23). The columns labeled *I* and *II* stand for the short-range and small-angle scatterings, respectively, and for (b) hard-wall, (c) parabolic and (d) stepped QWs depicted in Fig. 1. $\hbar\kappa = \sqrt{2m(\varepsilon_{21} - \varepsilon_w)}$ with $\varepsilon_w = 2(\pi\hbar/d_w)^2/m$, $\kappa d_n \ll 1$, $\kappa d_w \gg 1$, and $q_0 d_w \ll 1$ and $a \approx 4.6 \times 10^{-3}$.

	<i>I</i> (b)	<i>I</i> (c)	<i>I</i> (d)	<i>II</i> (b)	<i>II</i> (c)	<i>II</i> (d)
K_{11}	$3/(2d)$	$1/(\sqrt{2}\pi\ell_{\perp})$	$\kappa/2$	$q_0/(2\sqrt{\pi})$	$q_0/(2\sqrt{\pi})$	$q_0/(2\sqrt{\pi})$
K_{22}	$3/(2d)$	$3/(4\sqrt{2}\pi\ell_{\perp})$	$3/(2d_w)$	$q_0/(2\sqrt{\pi})$	$q_0/(2\sqrt{\pi})$	$q_0/(2\sqrt{\pi})$
K_{12}	$1/d$	$1/(2\sqrt{2}\pi\ell_{\perp})$	$4\pi^2/[d_w(\kappa d_w)^2]$	$aq_0(q_0 d)^2$	$q_0(q_0\ell_{\perp})^2/(8\sqrt{\pi})$	$32\pi^{3/2}q_0^3/[\kappa^2(\kappa d_w)^3]$

FIGURE CAPTIONS

FIG. 1. (a) Schematic views of the spatial variations of two occupied energy levels in the QW along the x direction with (solid curve) and without (dotted curve) screening. Band diagrams for (b) hard-wall, (c) parabolic and (d) stepped QWs with non-ideal heterointerfaces.

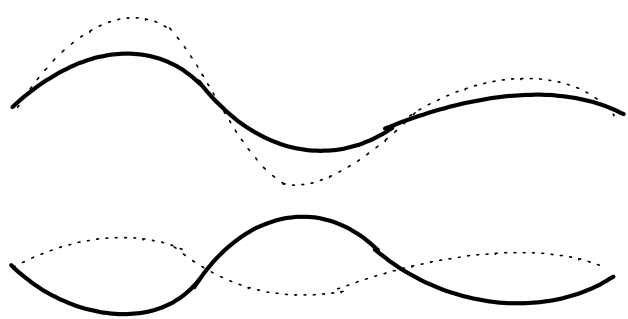
FIG. 2. Magnetoresistance $\Delta\rho_{eff}$ as a function of the magnetic field for short-range scattering. The solid and dash-dotted curves plot $10 \times \Delta\rho_{eff}$ in case of parabolic QWs, $\nu_2/\nu_1 = 5/6$, with $\overline{\delta n}/n_1 = 0.2$ and $\overline{\delta n}/n_1 = 0$, respectively. The dotted and dashed curves correspond to stepped QWs, $\nu_2/\nu_1 = 1/2.1$, with $\overline{\delta n}/n_1 = 0.2$ and $\overline{\delta n}/n_1 = 0$, respectively. The ratio between average subband populations $n_2/n_1 = 1/2$ and $\overline{\delta n}$ is the typical value of the concentration fluctuations in both occupied subbands.

FIG. 3. Hall coefficient R_{eff} as function of magnetic field for short-range scattering, where $R_0 = 1/ecn$, $n = n_1 + n_2$. The curves represent the same cases as pertinent curves in Fig. 2.

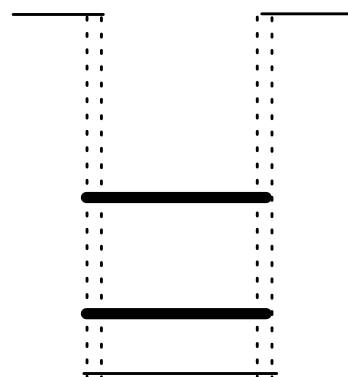
FIG. 4. Magnetoresistance $\Delta\rho_{eff}$ as function of magnetic field for small-angle scattering. The solid and dashed curves correspond to $n_2/n_1 = 1/2$ with $\overline{\delta n}/n = 1/8$ and $\overline{\delta n}/n = 0$, respectively. For comparison with the $\Delta\rho_{eff}$ behavior for short-range scattering, the dotted curve is the same as in Fig. 2.

FIG. 5. Hall coefficient R_{eff} as function of magnetic field for small-angle scattering. The solid, dashed, and dotted curves correspond to pertinent curves in Fig. 4.

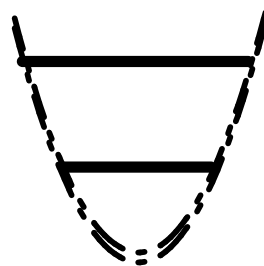
FIG. 6. Conductivity $\Delta\sigma^{eff}$, for zero magnetic field, as a function of $\Delta n = n_1 - n_2$ showing the effect of intersubband population redistribution due to transverse electric field. The solid and dot-dot-dashed curves, with a positive slope, are for small-angle scattering and $\overline{\delta n}/n = 1/8$ and $\overline{\delta n}/n = 0$, respectively. The thin solid (parabolic QW with $\overline{\delta n}/n = 0$) dotted (stepped QW with $\overline{\delta n}/n = 1/8$), and dashed curves (stepped QW with $\overline{\delta n}/n = 0$) are for short-range scattering; other parameters are the same as for the stepped QW in Fig. 2.



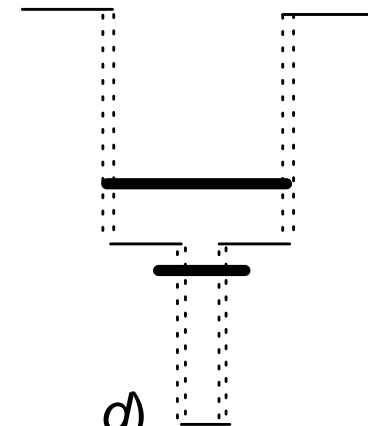
a)



b)



c)



d)

Fig.1

O.G.Balev *et al.*

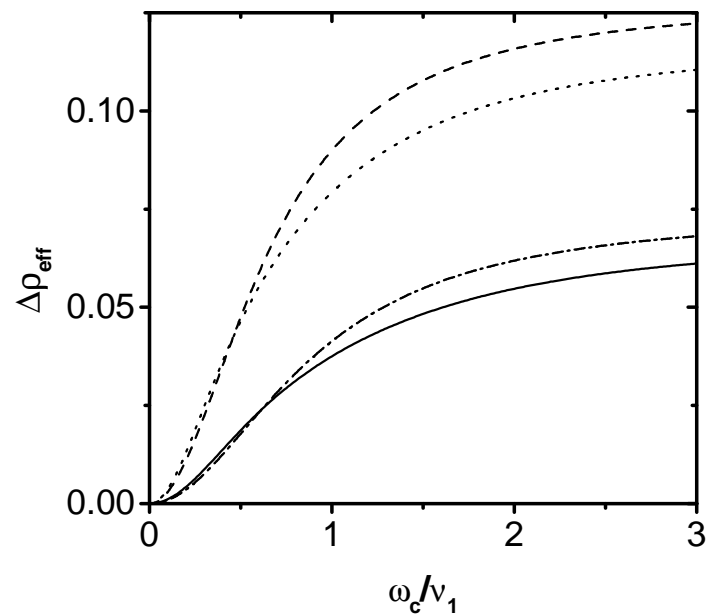


Fig. 2

O. G. Balev *et al.*,

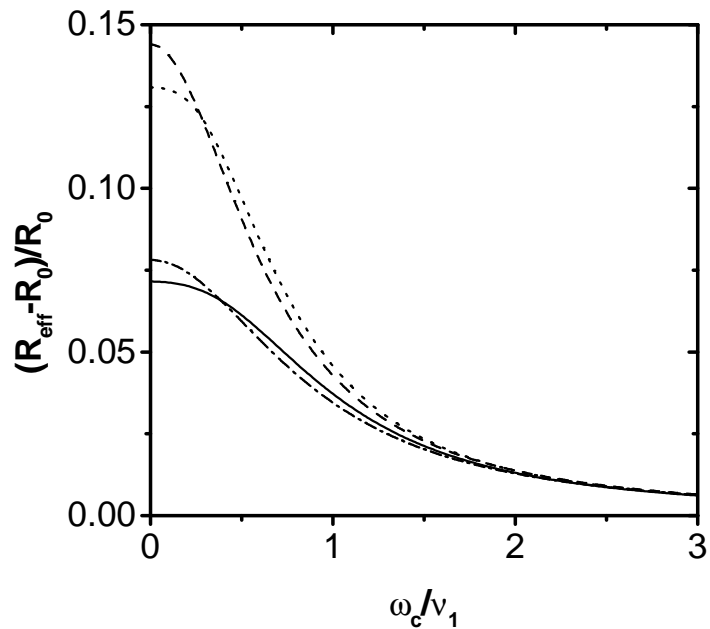


Fig. 3

O. G. Balev *et al.*,

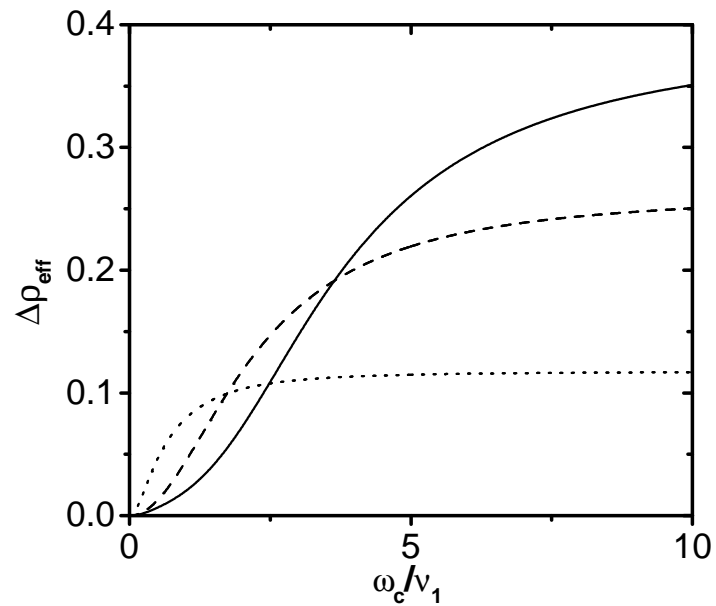


Fig. 4,
O. G. Balev *et al.*,

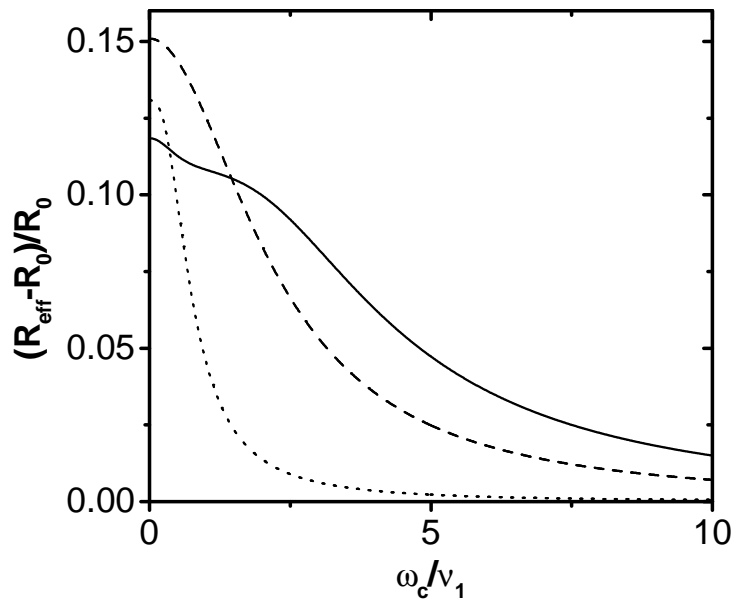


Fig. 5,
O. G. Balev *et al.*,

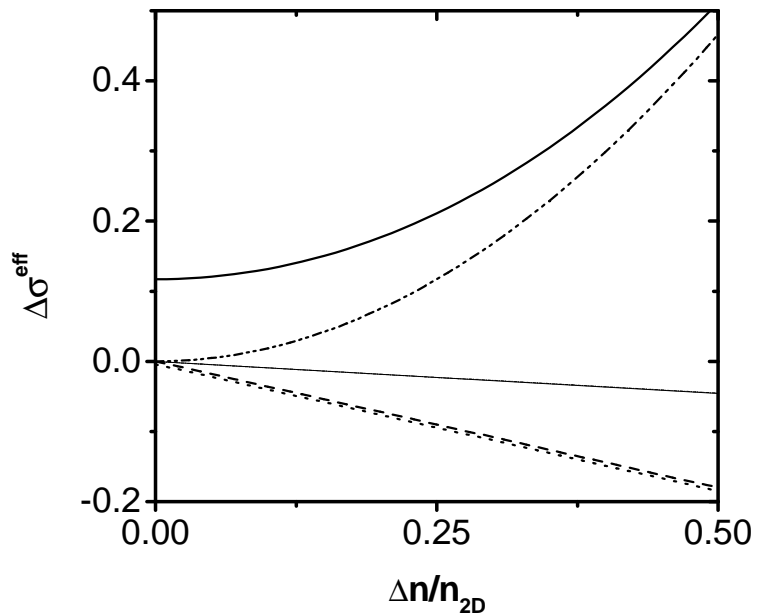


Fig. 6.

O. G. Balev *et al.*,